Low-Dose Bone Morphogenetic Protein-2/Stromal Cell-Derived Factor-1β Cotherapy Induces Bone Regeneration in Critical-Size Rat Calvarial Defects

Samuel Herberg, PhD,[1,2] Cristiano Susin, DDS, MSD, PhD,[3–5] Manuel Pelaez, DMD, MS,[3] R. Nicole Howie, MS,[4] Rubens Moreno de Freitas, DDS,[3] Jaebum Lee, DDS, MSD, PhD,[3,4] James J. Cray, Jr., PhD,[4,5] Maribeth H. Johnson, M.,[6] Mohammed E. Elsalanty, MD, PhD,[4,7] Mark W. Hamrick, PhD,[2,5,7,8] Carlos M. Isales, MD,[2,5,7,8] Ulf M.E. Wikesjö, DDS, DMD, PhD,[3–5,7] and William D. Hill, PhD[1,2,5,7,8]

Increasing evidence suggests that stromal cell-derived factor-1 (SDF-1/CXCL12) is involved in bone formation, though underlying molecular mechanisms remain to be fully elucidated. Also, contributions of SDF-1β, the second most abundant splice variant, as an osteogenic mediator remain obscure. We have shown that SDF-1β enhances osteogenesis by regulating bone morphogenetic protein-2 (BMP-2) signaling *in vitro*. Here we investigate the dose-dependent contribution of SDF-1β to suboptimal BMP-2-induced local bone formation; that is, a dose that alone would be too low to significantly induce bone formation. We utilized a critical-size rat calvarial defect model and tested the hypotheses that SDF-1β potentiates BMP-2 osteoinduction and that blocking SDF-1 signaling reduces the osteogenic potential of BMP-2 *in vivo*. In preliminary studies, radiographic analysis at 4 weeks postsurgery revealed a dose-dependent relationship in BMP-2-induced new bone formation. We then found that codelivery of SDF-1β potentiates suboptimal BMP-2 (0.5 μg) osteoinduction in a dose-dependent order, reaching comparable levels to the optimal BMP-2 dose (5.0 μg) without apparent adverse effects. Blocking the CXC chemokine receptor 4 (CXCR4)/SDF-1 signaling axis using AMD3100 attenuated the osteoinductive potential of the optimal BMP-2 dose, confirmed by qualitative histologic analysis. In conclusion, SDF-1β provides potent synergistic effects that support BMP-induced local bone formation and thus appears a suitable candidate for optimization of bone augmentation using significantly lower amounts of BMP-2 in spine, orthopedic, and craniofacial settings.

Introduction

BONE MORPHOGENETIC PROTEINS (BMPs) comprise a cluster of phylogenetically highly conserved proteins constituting the largest subgroup of the transforming growth factor-β (TGF-β) superfamily. Discovered in the 1960s,[1] purified and sequenced in the late 1980s, recombinant forms became available for preclinical and clinical evaluations in the 1990s.[2–4] To date over 20 members of the BMP family have been identified and characterized. BMP signals are transduced through a functional complex of type I/II BMP receptors resulting in the phosphorylation of receptor-regulated Smad1/5/8. These Smad proteins then complex with the common partner protein Smad4 and translocate into the nucleus to regulate gene expression.[5] In addition, BMP receptors can activate non-Smad pathways, such as p38 MAPK and JNK.[6] Numerous preclinical and several randomized clinical trials have demonstrated the safety and efficacy of BMPs in support of local bone formation in the axial[7–9] and appendicular[10–13] skeleton. However, side effects and aberrant events, including critical soft tissue inflammation/swelling and ectopic bone formation, in particular, with off-label use, have been linked to the high-dose commercial BMP product and evoked controversy.[10,14,15] Thus, considerable efforts are being pursued to enhance our understanding of BMP biology to ultimately improve and expand clinical utility.

Stromal cell-derived factor-1 (SDF-1), also known as CXCL12, is a member of the proinflammatory CXC chemokine family.[16] SDF-1 and its cognate G-protein-coupled seven-transmembrane CXC chemokine receptor 4 (CXCR4) are expressed in various tissues.[17–19] Binding of SDF-1 to CXCR4 initiates diverse downstream signaling processes,[20] including the recruitment of regenerative cells to injury sites during the acute phase of bone repair.[21–23] Moreover, a direct regulatory role for SDF-1 signaling in BMP-2 osteogenic differentiation of C2C12 and ST2 cells, mediated through intracellular Smads and MAPK activation, has been reported.[24] These *in vitro* findings were later extended using primary mouse and human bone-marrow-derived mesenchymal stem cells (BMSCs),[25] setting the stage for investigating the BMP-2/SDF-1 interaction employing orthotopic and ectopic bone formation models.[26–29]

Previous studies have suggested that the CXCR4/SDF-1 axis functions in postnatal bone formation by regulating osteoblast development in cooperation with BMP signaling, and that CXCR4 acts as an endogenous signaling component necessary for bone formation.[29] We[30] and others[31] have shown that bone marrow endothelial and stromal cells, and osteoblasts express both major SDF-1 splice variants, and that unexpectedly the beta isoform may be present at a high level in bone tissues.[31] We have also shown that, independent of SDF-1α, SDF-1β enhances BMP-2-stimulated mineralization, mRNA and protein expression of key osteogenic markers, regulates BMP-2 signal transduction via Erk1/2 phosphorylation, and promotes the migratory response of CXCR4-expressing BMSCs *in vitro*,[30] suggesting an SDF-1β autocrine and paracrine activity. An important characteristic of SDF-1β is its protection from proteolytic cleavage at the C-terminus, distinguishing SDF-1β from SDF-1α. Further, the four additional C-terminal amino acids are thought to mediate SDF-1β cell and extracellular stability, increasing its half-life and potency in vascularized tissues.[32–34] This raises the possibility that SDF-1β may primarily be involved in targeting cells to areas of need and during regenerative processes while SDF-1α may be more important acting as a short-lived signaling molecule.

Given the prospect of improved interaction of BMP-2 and SDF-1β due to its previously unappreciated association with bone, we investigated dose-dependent contributions of SDF-1β to suboptimal BMP-2 utilizing a critical-size rat calvarial defect model and tested the hypotheses that SDF-1β potentiates BMP-2 osteoinduction and that blocking SDF-1 signaling reduces the osteogenic potential of BMP-2.

Materials and Methods

Animals

One hundred seventy-two, 11–13-week-old, male Sprague-Dawley rats (Harlan Laboratories, Indianapolis, IN) were used. The animals were maintained at the Laboratory Animal Services research facility at Georgia Regents University. The animals had *ad libitum* access to water and a standard laboratory diet throughout the study. All aspects of the research were conducted in accordance with the guidelines set by the local Institutional Animal Care and Use Committee following an approved protocol.

Experiments and study groups

Since optimal and suboptimal doses for BMP-2 have not been established for the critical-size calvarial defect model, we devised a preliminary study to test escalating doses of BMP-2. Seventy-two animals randomized into nine groups of eight each received 0.1, 0.5, 1.3, 2.5, 5, 10, or 20 μg BMP-2 (recombinant human BMP-2; INFUSE™ Bone Graft; Medtronic, Memphis, TN) soak-loaded onto an absorbable collagen sponge (ACS; Helistat, Integra Life Sciences, Plainsboro, NJ) carrier. Controls included sham-surgery and ACS soak-loaded with saline.

For the main study, 100 animals were randomized into 10 groups of 10 each. We evaluated suboptimal BMP-2 (0.5 μg) alone and codelivered with increasing doses of SDF-1β (rhSDF-1β; 1–60 μg; PeproTech, Rocky Hill, NJ). Optimal BMP-2 (5.0 μg) was used alone and codelivered with the CXCR4 antagonist AMD3100 {1,1′-[1,4-phenylenebis (methylene)]-*bis*-1,4,8,11-tetraazacyclotetradecane octahydrochloride; 1750 μg (equivalent to a 5.0-mg/kg single dose); Tocris Bioscience, Ellisville, MO}, with and without additional SDF-1β (15 μg). Controls included saline, SDF-1β, and AMD3100 (Table 1).

Critical-size calvarial defect model

The critical-size calvarial defect model was performed as described previously.[35] Animals were premedicated using buprenorphine (0.05–0.1 mg/kg; SC) and meloxicam (0.1–0.2 mg/kg; SC). Anesthesia was induced using a ketamine HCl (40 mg/kg; IP)/xylazine HCl (8 mg/kg; IP) cocktail. After induction, the dorsal surface of the head was shaved and disinfected using a 10% betadine solution. Animals were ear-punched, stabilized into a stereotaxic device (Stoelting Company, Wood Dale, IL) fitted with an anesthesia nose cone, and draped. Isoflurane (1.0%–3.0%) was administered to maintain a surgical plane of anesthesia. Using aseptic routines, a 3-cm midline incision was made through the skin along the sagittal suture of the skull (Fig. 1A–L). Soft tissues and periostea were elevated and reflected. Under saline irrigation, a critical-size, 8-mm, through-through, calvarial osteotomy defect centered over the sagittal suture immediately anterior to the occipital suture was created without disrupting the underlying dura mater using a diamond-coated trephine (Continental Diamond Tool, New Haven, IN).

The defects received an 8-mm precut ACS soak-loaded (22% saturation) with respective treatments and allowed to set for 15 min prior to implantation. After the ACS constructs were inserted into the defect, a sterile custom, dome-shaped titanium micromesh (Jeil Medical, Seoul, Korea) was placed over the defect to prevent soft tissue collapse/compression. Finally, the flaps were adapted and closed ensuring everted wound margins using surgical staples (Visistat, Teleflex Medical, London, United Kingdom). Animals were placed in cages, warmed on a heating pad, and observed for distress until freely moving about. Yohimbine HCl (1–2 mg/kg; IP) was administered for xylazine reversal. The animals received meloxicam (0.1–0.2 mg/kg; SC) every 24 h for 48 h for pain control. They were euthanized at 4 weeks using CO_2 asphyxiation followed by thoracotomy and decapitation. Skulls were fixed in 3% paraformaldehyde. After 5 days, block biopsies

TABLE 1. TREATMENT GROUPS AND DOSE (µG)

	BMP-2	BMP-2+SDF-1β (1)	BMP-2+SDF-1β (5)	BMP-2+ SDF-1β (15)	BMP-2+ SDF-1β (60)
Suboptimal BMP-2 dose					
BMP-2	0.5	0.5	0.5	0.5	0.5
SDF-1β	0	1	5	15	60

	BMP-2	BMP-2+AMD3100	BMP-2+AMD3100+ SDF-1β		
Optimal BMP-2 dose					
BMP-2	5	5	5		
SDF-1β	0	0	15		
AMD3100	0	1750	1750		

|	Saline	SDF-1β	AMD3100		
Controls					
BMP-2	0	0	0		
SDF-1β	0	15	0		
AMD3100	0	0	1750		

BMP-2, bone morphogenetic protein-2; SDF-1, stromal cell-derived factor-1.

$(12 \times 15 \, mm^2)$ of the calvariae were harvested using a diamond drill (New Technology Instruments, Kahla, Germany), washed in phosphate-buffered saline, and preserved in 70% ethyl alcohol at 4°C, the titanium mesh and overlying soft tissue being removed.

Radiographic analysis

Calvarial specimens were placed in 100-mm cell culture dishes and radiographed using a digital imaging instrument (Faxitron X-Ray, Wheeling, IL) following initial calibration.

FIG. 1. Critical-size calvarial defect model. Clinical series showing (A) rat stabilized in the stereotaxic frame fitted with an anesthesia nose cone, (B) a 3-cm midline incision through the skin along the sagittal suture of the skull, (C) elevated and reflected soft tissues and periostea, (D–H) creation of a critical-size, 8-mm, through-through, cranial defect centered over the sagittal suture immediately anterior to the occipital suture using a diamond-coated trephine bur without disrupting the underlying dura mater, (I) implanted defect with 8-mm precut absorbable collagen sponge soak-loaded with the respective treatment, (J) placement of a custom, dome-shaped titanium micromesh to avoid soft tissue collapse/compression into the defect, and (K, L) adapted and closed flaps using surgical staples to ensure everted wound margins. Color images available online at www.liebertpub.com/tea
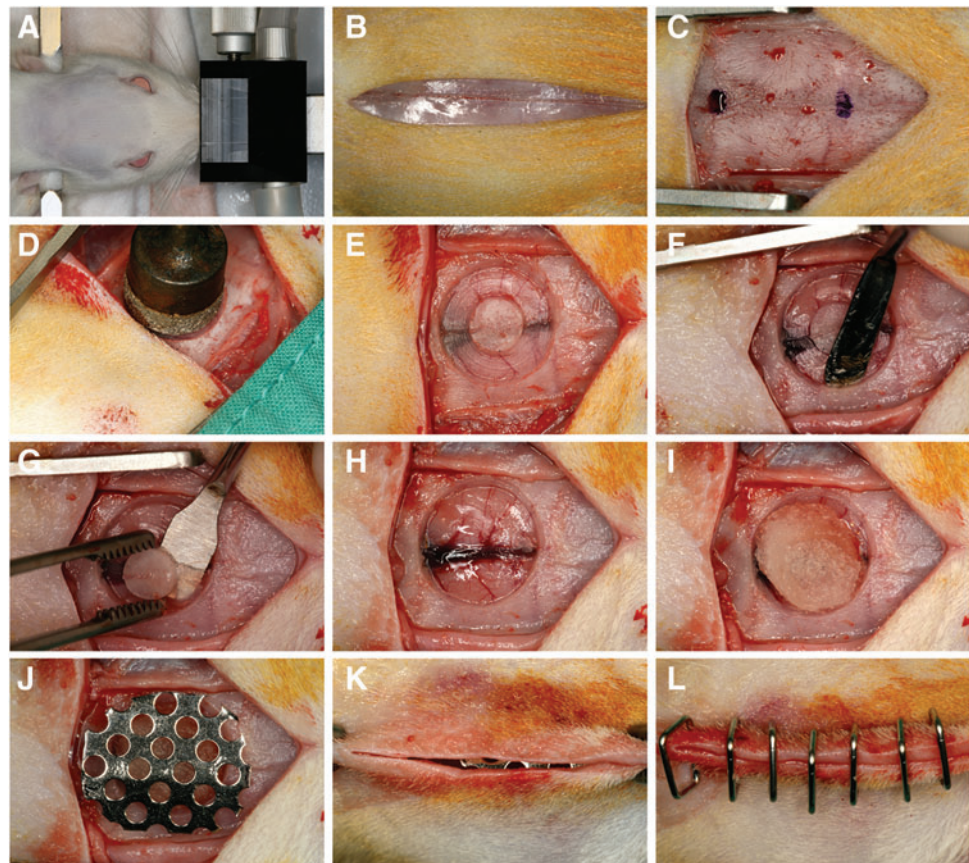
Relative radiographic bone density (histogram raw values) for each defect was estimated using a 7.5-mm region of interest (ROI) and Photoshop CS4 v11.0 software (Adobe Systems, San Jose, CA).

Microcomputed tomography (μCT)

Calvarial specimens derived from the main study were scanned using an *ex vivo* microcomputed tomography (μCT) system (Skyscan 1174; Skyscan, Aartlesaar, Belgium). The scanner was equipped with a 50-kV, 800 μA X-ray tube and a 1.3 megapixel CCD coupled to a scintillator. Each sample was placed in a sample holder with the sagittal suture oriented parallel to the image plane and scanned in air using 18-μm isotropic voxels, 400 ms integration time, 0.5° rotation step, 360° rotation, and frame averaging of 5. For 3D reconstruction (NRecon software; Skyscan), the gray scale was set from 60 to 220. Standard 3D morphometric parameters[36] (CTAn software; Skyscan) were determined in the ROI (7.5 mm; 65 cuts). For bone mineral density (BMD) measurements using the same ROI, calibration was performed with 0.25 and 0.75 mg/cc hydroxyapatite phantoms (provided by the manufacturer). Representative 3D images were created using CTvox software (Skyscan).

Histological preparation and analysis

Calvarial specimens were decalcified in 0.25 M ethylenediaminetetraacetic acid (EDTA) at pH 7.4 for 7 days at 4°C with changes of the EDTA solution every other day. Specimens were washed, dehydrated in a graded series of ethyl alcohol (70%–100%), cleared in xylene, embedded in paraffin parallel to the sagittal suture (through the center of the defect), sectioned using a microtome (Leica Microsystems, Buffalo Grove, IL) set at 8 μm, and mounted on Frost Plus glass slides. Serial sections were stained using standard H&E (Fisher Scientific, Kalamazoo, MI) and picrosirius red (Sigma-Aldrich, St. Louis, MO). Light microscopy images were captured using a Carl Zeiss microscope (Carl Zeiss, Thornwood, NY) and the AxioVision Image Analysis software (Carl Zeiss).

Statistical analysis

All data are expressed as mean ± SD. One-way analysis of variance followed by Tukey's *post hoc* test was used to determine mean differences between groups. The significance level was set at 5%. Data were analyzed using GraphPad Prism 5.0 software (GraphPad Software, La Jolla, CA).

Results

Preliminary study: suboptimal and optimal BMP-2

Radiographic images of the calvarial defects at 4 weeks suggested a dose-dependent increase in BMP-induced bone formation, plateauing at a BMP-2 dose of 5.0 μg followed by an apparent drop at higher doses (Fig. 2A). The
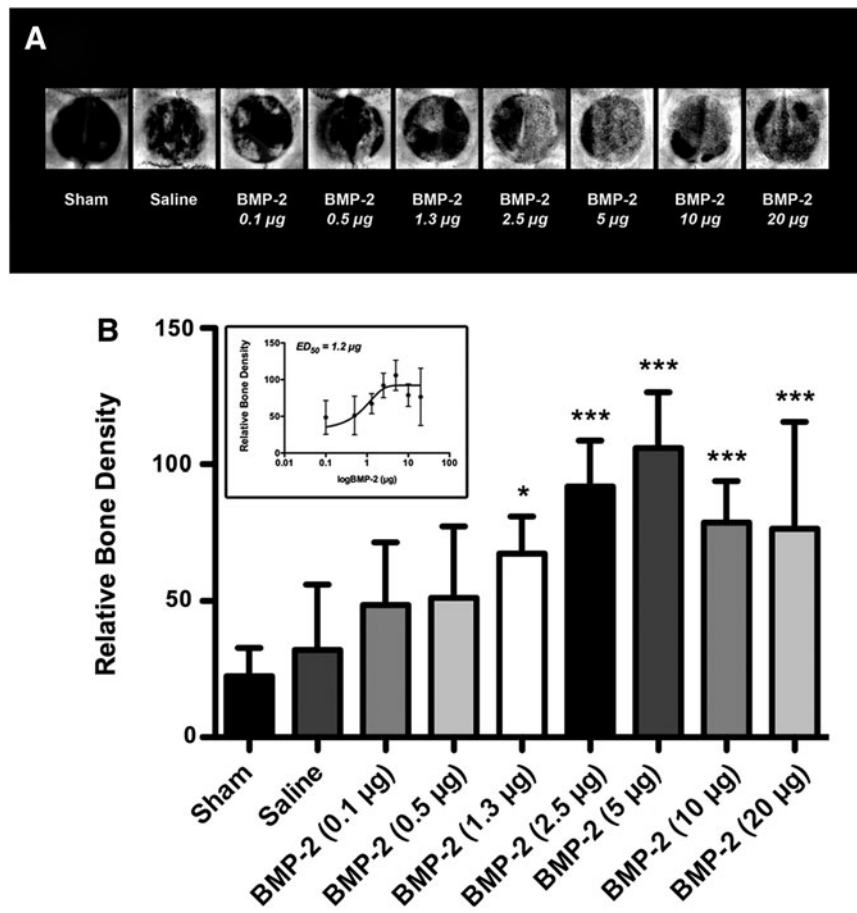

FIG. 2. Bone morphogenetic protein-2 (BMP-2) significantly induces bone formation in a dose-dependent order. **(A)** Representative radiographic images of critical-size rat calvarial defects at 4 weeks. **(B)** Quantitative analysis of the bone formation within the craniotomy defect revealed dose-dependent significantly increased relative bone densities compared with saline control, reaching a plateau at 5.0 μg followed by a trend of reduced bone formation with increasing doses, with a half-maximal effective BMP-2 dose (ED$_{50}$; inset) of 1.2 μg (*$p < 0.05$, ***$p < 0.0001$ vs. saline control; $n = 8$ animals/group).

quantitative analysis concurred with the qualitative estimate showing a dose-dependent increase in relative bone density compared with saline control, with a half-maximal effective BMP-2 dose (ED_{50}) of 1.2 µg ($p < 0.05$; $p < 0.0001$; Fig. 2B, inset). Therefore, suboptimal BMP-2 in this model was defined as being lower than the ED_{50}, while optimal BMP-2 was established as no higher than 5.0 µg due to a plateau effect.

Radiographic and µCT analyses

Based on these findings, suboptimal BMP-2 (0.5 µg) was given alone or codelivered with increasing doses of SDF-1β (1–60 µg), while optimal BMP-2 (5.0 µg) was used alone or codelivered with the CXCR4 antagonist AMD3100 (1750 µg), with and without SDF-1β (15 µg). Quantitative radiographic analysis of the newly formed bone within the craniotomy defect showed significantly increased relative bone densities in suboptimal BMP-2/SDF-1β groups compared with saline control, reaching comparable levels to the optimal BMP-2 dose ($p < 0.05$; $p < 0.01$; Supplementary Fig. S1B; Supplementary Data are available online at www.liebertpub.com/tea). Importantly, SDF-1β (15 and 60 µg) significantly enhanced the suboptimal BMP-2 osteoinduction ([a]$p < 0.05$; Supplementary Fig. S1B). Codelivery of AMD3100 attenuated optimal BMP-2 bone formation ([#]$p < 0.05$; Supplementary Fig. S1B). AMD3100 and SDF-1β controls performed similar to saline controls (Supplementary Fig. S1B).

We next employed *ex vivo* µCT to further characterize bone formation in more detail. Representative 3D reconstructions at 4 weeks postsurgery are depicted in Figure 3. Quantitative analyses of standard 3D bone morphometric parameters revealed significantly increased percent bone volume (BV/TV) and BMD with the addition of 15 µg or 60 µg SDF-1β compared with suboptimal BMP-2 alone ([a]$p < 0.05$; Fig. 4). Trabecular number (Tb.N) was significantly increased in these two groups relative to lower doses of SDF-1β ([a]$p < 0.05$; Table 2), while trabecular thickness (Tb.Th) was significantly decreased ([b]$p < 0.01$; Table 2). Trabecular separation (Tb.Sp) was markedly reduced with SDF-1β cotherapy but did not reach significance (Table 2). In summary, SDF-1β cotherapy (15 and 60 µg) significantly enhanced suboptimal BMP-2-induced new bone formation. Codelivery of AMD3100 significantly attenuated the osteoinductive potential of optimal BMP-2 (BV/TV) indicative of the critical importance of the CXCR4/SDF-1 signaling axis and specifically the potential of SDF-1β in BMP-2-mediated bone formation ([#]$p < 0.05$; Fig. 4). Tb.N and BMD reflected the alterations in BV/TV. Both AMD3100 and SDF-1β controls were comparable to saline control (BV/TV, Tb.N, Tb.Th, Tb.Sp, and BMD) (Fig. 4 and Table 2). Of note, no synergistic effect of SDF-1β cotherapy (1–15 µg) was observed when combined with the optimal BMP-2 dose (5.0 µg) employing both radiographic and µCT analyses (data not shown).

Histology

Qualitative histologic analysis mirrored the 2D and 3D microstructural bone evaluation within the craniotomy defect. Sites receiving saline control showed large amounts of residual ACS invested in fibrovascular tissue and bone (data not shown). No noticeable differences were observed compared with SDF-1β and AMD3100 controls (data not shown). Further, only limited bone formation emerging from the defect margins comparable to saline control was seen with suboptimal BMP-2 (Fig. 5A). Internal and

FIG. 3. Stromal cell-derived factor-1 (SDF-1)β enhances suboptimal BMP-2. **(A)** Representative 3D reconstruction of micro-computed tomography images at 4 weeks, in agreement with radiographic observations, confirm limited bone formation using suboptimal BMP-2 compared with saline control. Importantly, a dose-dependent potentiation (1–60 µg) of suboptimal BMP-2-induced bone formation was observed with SDF-1β cotherapy, reaching comparable levels to the benchmark optimal BMP-2. **(B)** Codelivery of the specific CXC chemokine receptor 4 (CXCR4) antagonist AMD3100 with optimal BMP-2 attenuated the osteoinductive potential. Neither of the control groups showed signs of significant bone formation ($n = 10$ animals/group).
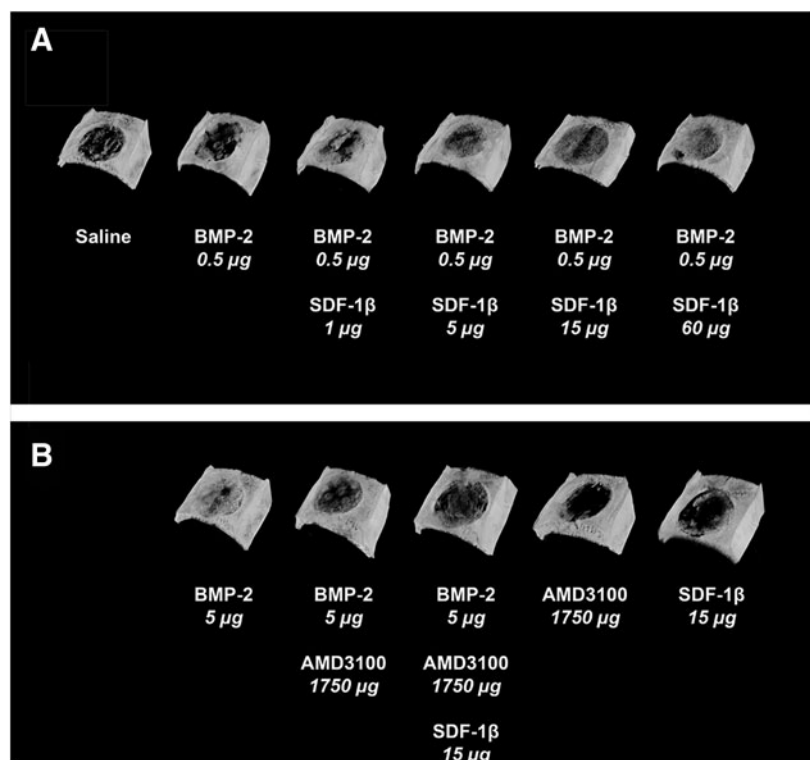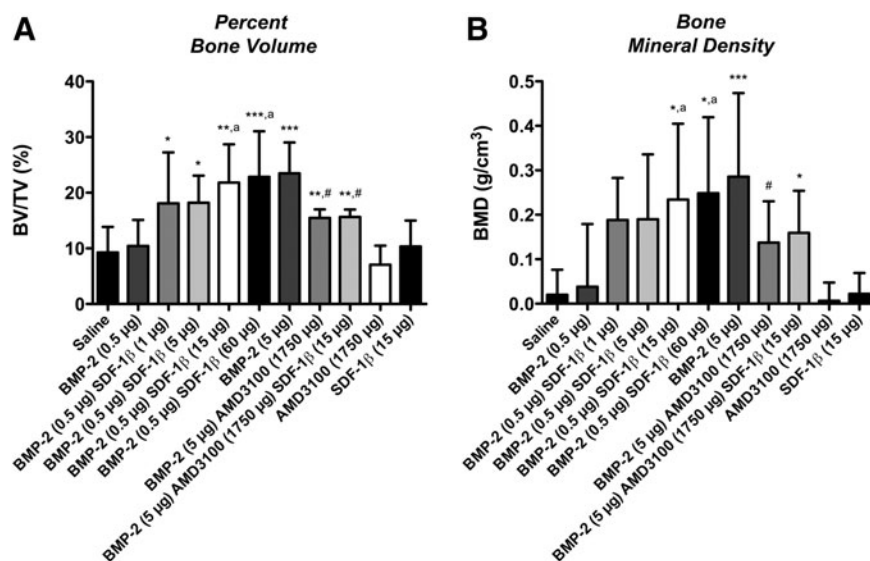
FIG. 4. SDF-1β significantly potentiates suboptimal BMP-2-induced bone formation and allows for optimal BMP-2 signaling following local codelivery. Three-dimensional bone morphometry parameters **(A)** percent bone volume (BV/TV) and **(B)** bone mineral density (BMD) within the craniotomy defect revealed limited bone formation using suboptimal BMP-2 alone, similar to saline control. Importantly, SDF-1β significantly enhanced suboptimal BMP-2-induced bone formation in a dose-dependent fashion (1–60 μg), reaching comparable levels to the benchmark optimal BMP-2 with codelivery of 15 or 60 μg SDF-1β [*$p < 0.05$, **$p < 0.01$, ***$p < 0.0001$ vs. saline control; [a]$p < 0.05$ vs. BMP-2 (0.5)]. Codelivery of the specific CXCR4 antagonist AMD3100 with optimal BMP-2 mitigated both BV/TV and BMD seen with optimal BMP-2 alone [**$p < 0.01$ vs. saline control; [#]$p < 0.05$ vs. BMP-2 (5.0)]. Neither of the control groups showed signs of significant bone formation ($n = 10$ animals/group).

external cortical plates were partially restored with bone formation ranging from woven to lamellar bone (Fig. 5A1, A2); complete bone fill was observed only in few sites. In contrast, a dose-dependent potentiation of suboptimal BMP-2-induced bone formation was observed following SDF-1β cotherapy. Importantly, codelivery of 15 or 60 μg SDF-1β and suboptimal BMP-2 reached bone formation levels similar to the 10-fold greater optimal BMP-2 with a greater fraction lamellar/woven bone relative to suboptimal BMP-2 alone (as shown by picro-sirius red staining for collagen; lamellar = , woven = *), suggesting SDF-1β-driven accelerated bone maturation (Fig. 5B1, B2). Defect sites receiving optimal BMP-2 showed robust bone formation. The internal and external cortical plates were frequently reestablished within 4 weeks including trabecular bone with cell-rich fibrovascular and fatty marrow (Fig. 5C1, C2). Perturbing the CXCR4 signaling axis using AMD3100 attenuated the osteoinductive potential of optimal BMP-2, irrespective of the presence of exogenous SDF-1β (data not shown). Collectively, the data suggest that SDF-1 signaling is pivotal for BMP-2-induced bone formation and maturation.

Discussion

Based on evidence that the CXCR4/SDF-1 signaling axis is critical in mediating BMP-2 function and that SDF-1β is expressed in bone tissues, we sought to determine whether BMP-2/SDF-1β cotherapy would permit the use of a significantly reduced BMP-2 dose in driving bone formation. As such, the objective of this study was to determine the effect of SDF-1β on suboptimal BMP-2 osteoinduction using a critical-size rat calvarial defect model. We hypothesized that SDF-1β potentiates BMP-2-induced bone formation and that blocking SDF-1 signaling reduces the osteogenic potential of BMP-2. Our results demonstrated that SDF-1β permits osteoinduction with very low, suboptimal, levels of BMP-2 that alone do not significantly induce bone formation. Specifically, we showed that SDF-1β potentiates suboptimal BMP-2 osteoinduction in a dose-dependent order reaching comparable levels to the 10-fold higher optimal BMP-2 dose without apparent side effects. Blocking the CXCR4/SDF-1 signaling axis blunted BMP-2-mediated bone formation. This suggests that SDF-1, in particular the beta isoform, is of interest in translational approaches to enhance bone formation via the BMP-2 pathway and may permit low-dose clinical BMP-2 therapies with reduced negative side effects.[10,14] Coadministration of SDF-1β locally has the additional potential value of inducing angiogenesis and attracting circulating osteogenic progenitor cells to the defect site.[21–23] Normal SDF-1 release from injury sites is involved in mobilization of reparative cells from their niches, as well as their homing to the injury site.[37] Therefore, delivery of additional exogenous SDF-1 to the repair site would be expected to amplify its normal role. While SDF-1 mediates stem cell and leukocyte mobilization and homing as part of inflammatory responses, its activity is tightly regulated temporally and spatially. This occurs in large part via proteolysis and scavenging, which limits biologically active SDF-1.[37] Importantly, the safety of delivery of even high doses of SDF-1 to injury sites in humans is supported by a recent clinical trial.[38] Localized delivery of SDF-1-expressing plasmids to the injured myocardium was

TABLE 2. MICROCOMPUTED TOMOGRAPHY 3D BONE MORPHOMETRY (MEAN ± SD)

	Saline (0.5)	BMP-2 (0.5)	BMP-2 (0.5) SDF-1β (1)	BMP-2 (0.5) SDF-1β (5)	BMP-2 (0.5) SDF-1β (15)	BMP-2 (0.5) SDF-1β (60)	BMP-2 (5)	BMP-2 (5) AMD3100 (1750)	BMP-2 (5) AMD3100 (1750) SDF-1β (15)	AMD3100 (1750)	SDF-1β (15)
Tb.N (1/mm)	0.4 ± 0.2	0.5 ± 0.3	0.8 ± 0.3	0.9 ± 0.4*	1.1 ± 0.4***,a	1.1 ± 0.3***,a	1.3 ± 0.3***	1.0 ± 0.1***,#	1.1 ± 0.1***	0.3 ± 0.1	0.5 ± 0.2
Tb.Th (mm)	0.22 ± 0.03	0.23 ± 0.03	0.23 ± 0.04	0.19 ± 0.03ᵃ	0.18 ± 0.03ᵇ	0.17 ± 0.02*,b	0.17 ± 0.02***	0.15 ± 0.01***	0.15 ± 0.01***	0.22 ± 0.04	0.21 ± 0.02
Tb.Sp (mm)	1.17 ± 0.33	1.25 ± 0.34	0.99 ± 0.21	0.96 ± 0.39	0.85 ± 0.43	0.83 ± 0.26	0.65 ± 0.14***	0.55 ± 0.06***	0.55 ± 0.07***	1.42 ± 0.21	1.22 ± 0.35

*p < 0.05; ***p < 0.0001 versus saline control; ᵃp < 0.05; ᵇp < 0.01 versus BMP-2 (0.5); #p < 0.05 versus BMP-2 (5.0); n = 10 animals per group.
Tb.N, trabecular number; Tb.Th, trabecular thickness; Tb.Sp, trabecular separation.

shown to reduce the infarction via recruitment of reparative cells and induction of angiogenesis without significant negative side effects.[38]

Previous studies have suggested that the CXCR4/SDF-1 signaling axis regulates BMP-2 osteoinduction *in vitro*[24,25] and *in vivo*.[21–23,26–29] However, clear distinctions between involved SDF-1 isoforms were not reported. Thus, the specific contribution of SDF-1β, the second most abundant splice variant, to BMP-2-induced bone formation remained unknown. In previous studies, we showed that SDF-1β enhances BMP-2-induced osteogenic differentiation of CXCR4-expressing BMSCs *in vitro*[30] and *in vivo* (unpublished) in addition to regulating BMSC survival under oxidative stress through increasing autophagy.[39] Therefore, we hypothesized that SDF-1β would potentiate BMP-2-induced bone formation *in vivo* using an established animal model of acute bone injury.

Several animal platforms and defect models have been used to screen candidate osteoconductive and osteoinductive technologies prior to pivotal evaluation in discriminating large-animal models and ultimately clinical settings. The rat critical-size calvarial defect model[35,40–42] has allowed substantial progress in tissue engineering and regenerative medicine, setting the stage for numerous preclinical and clinical studies, which showed the powerful potential of BMP-2/7 in accelerating bone regeneration and fracture healing.[10–13,42] Advantages of the rat calvarial defect model include limited morbidity and mortality, shortened experimental periods, easy histologic and radiographic analyses, highly reproducible technique, and reduced cost. Nevertheless, caution should be exercised when extrapolating findings from this model to endochondral bone formation and load-bearing sites. In this regard, even though limited functional loading should be expected in the calvaria, the carrier still needs structural integrity to counteract soft tissue collapse into the defect or compression due to intracranial pressure. We used a 10-mm, dome-shaped titanium mesh to ensure space provision since the ACS carrier would not be able to withstand local demands. Previous studies from our laboratory have shown that bone formation can be negatively affected due to the collapse of soft tissue (or soft tissue infiltration) into the calvaria defect when a space-providing device is not used in this animal model.[40]

In a preliminary study, we first attempted to clarify the dose effect of BMP-2 soak-loaded onto an ACS carrier. We found a dose-dependent relationship in BMP-2-induced new bone formation utilizing quantitative radiographic analysis. In our model, suboptimal BMP-2 doses were defined as lower than the ED_{50} of 1.2 μg, while the optimal dose was determined as no higher than 5.0 μg due to a plateau effect using higher doses. Previous studies from our research group using canine[43,44] and non-human primate[45] models demonstrated that comparatively higher BMP-2 doses are associated with delayed bone maturation in craniofacial settings. This finding appears explained by an increased local inflammatory response to higher doses of BMP-2, also evidenced by frequent seroma formation[46] and increased remodeling/resorption rates of the adjoining resident bone.[43–45] Importantly, over longer healing intervals, bone maturation obscures these effects. It is noteworthy to point out that, based on the manufacturer's recommendations, our study only used ∼0.5%–10% BMP-2 per implant compared with that of the commercial product. Given the numerous
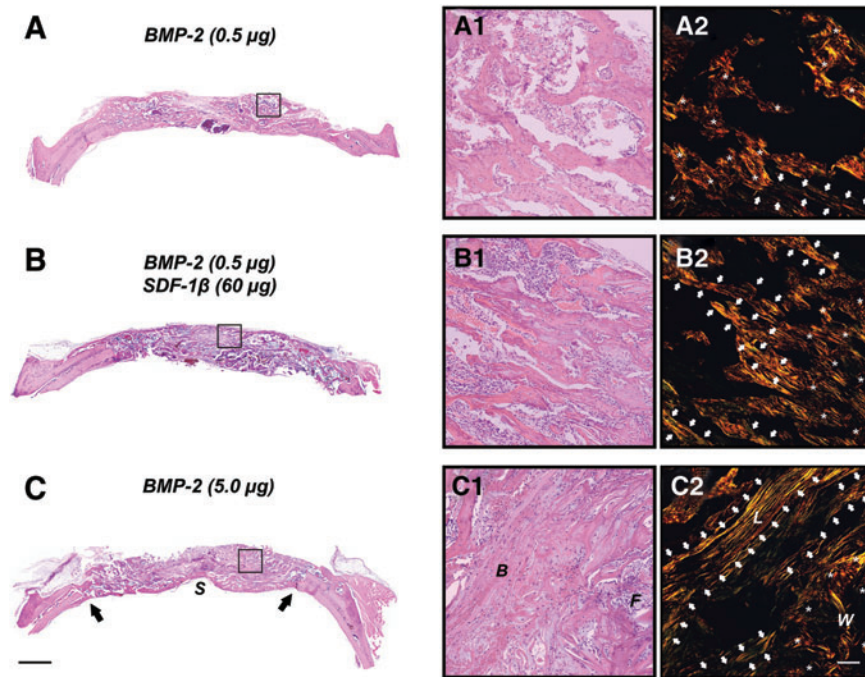
FIG. 5. SDF-1β enhances suboptimal BMP-2-induced bone formation and allows for optimal BMP-2 signaling following local codelivery. Representative H&E- and picro-sirius red-stained photomicrographs of the critical-size rat calvarial defects at 4 weeks. **(A)** Limited bone formation emerging from the defect margins was seen with suboptimal BMP-2. Internal and external cortical plates were partially restored with bone formation ranging from woven to lamellar bone **(A1, A2)**. **(B)** In contrast, codelivery of 60 μg SDF-1β and suboptimal BMP-2 reached bone formation levels similar to the 10-fold greater optimal BMP-2 with a greater fraction lamellar/woven bone relative to suboptimal BMP-2 alone **(B1, B2)**. **(C)** Defect sites receiving optimal BMP-2 showed robust bone formation. The internal and external cortical plates were frequently reestablished within 4 weeks including trabecular bone with cell-rich fibrovascular and fatty marrow **(C1, C2)** [2.5×, scale bar = 500 μm; 20×, scale bar = 100 μm; **(A1–C1)**: H&E, **(A2–C2)**: picro-sirius red (polarized light); S, sagittal sinus; arrows, defect margins; B, bone; F, fibrovascular tissue; L, lamellar = ⬆; W, woven = *; $n = 10$ animals/group]. Color images available online at www.liebertpub.com/tea

adverse effects reported with commercial, high-dose BMP-2 product, including significant inflammatory and immunogenic responses,[10,14] the opportunities to significantly reduce the locally applied BMP-2 dose for bone formation present an intriguing avenue for translational development.

Consequently, we next investigated the dose-dependent contribution of SDF-1β to a BMP-2 dose that was suboptimal for osteoinduction, using radiographic and μCT analyses. Codelivery of SDF-1β potentiated suboptimal 0.5 μg BMP-2-induced bone formation in a dose-dependent order, reaching comparable levels to the 10-fold greater optimal 5.0 μg BMP-2 using 15 and 60 μg SDF-1β without apparent adverse effects, projecting a translational potential. Blocking CXCR4/SDF-1 signaling using AMD3100 blunted the osteoinductive potential of the BMP-2, confirmed by the qualitative histological analysis. AMD3100, a bicyclam antagonist of CXCR4, was initially developed for selective inhibition of CXCR4-facilitated human immunodeficiency virus (HIV) entry into cells,[47] and later it was reported to mobilize hematopoietic stem cells by directly antagonizing the CXCR4-mediated sensing of the SDF-1 chemotactic gradient in bone marrow.[48] Our data demonstrate, for the first time, that SDF-1β plays a pivotal role in suboptimal BMP-2-induced bone formation and maturation through regulating CXCR4 signaling *in vivo*, extending previous reports[26–29] and confirming our earlier findings *in vitro*.[30]

The data presented here show that SDF-1β provides significant synergistic effects supporting BMP-2-induced local bone formation and thus appears a suitable candidate for optimization of bone augmentation in spine, orthopedic, and craniofacial settings. Future studies will focus on including longer observation time points to better assess the role of SDF-1β in bone maturation and the codelivery of BMP-2/SDF-1β using discriminating large-animal models.

Disclosure Statement

The authors have no conflict of interest.

References

1. Urist, M.R. Bone: formation by autoinduction. Science **150,** 893, 1965.
2. Luyten, F.P., Cunningham, N.S., Ma, S., Muthukumaran, N., Hammonds, R.G., Nevins, W.B., Woods, W.I., and Reddi, A.H. Purification and partial amino acid sequence of osteogenin, a protein initiating bone differentiation. J Biol Chem **264,** 13377, 1989.
3. Wozney, J.M. The bone morphogenetic protein family and osteogenesis. Mol Reprod Dev **32,** 160, 1992.
4. Wozney, J.M., Rosen, V., Celeste, A.J., Mitsock, L.M., Whitters, M.J., Kriz, R.W., Hewick, R.M., and Wang, E.A. Novel regulators of bone formation: molecular clones and activities. Science **242,** 1528, 1988.
5. Wan, M., and Cao, X. BMP signaling in skeletal development. Biochem Biophys Res Commun **328,** 651, 2005.
6. Nohe, A., Hassel, S., Ehrlich, M., Neubauer, F., Sebald, W., Henis, Y.I., and Knaus, P. The mode of bone morphogenetic protein (BMP) receptor oligomerization determines different BMP-2 signaling pathways. J Biol Chem **277,** 5330, 2002.
7. Boyne, P.J., Lilly, L.C., Marx, R.E., Moy, P.K., Nevins, M., Spagnoli, D.B., and Triplett, R.G. *De novo* bone induction by recombinant human bone morphogenetic protein-2 (rhBMP-2) in maxillary sinus floor augmentation. J Oral Maxillofac Surg **63,** 1693, 2005.
8. Fiorellini, J.P., Howell, T.H., Cochran, D., Malmquist, J., Lilly, L.C., Spagnoli, D., Toljanic, J., Jones, A., and Nevins, M. Randomized study evaluating recombinant human bone morphogenetic protein-2 for extraction socket augmentation. J Periodontol **76,** 605, 2005.
9. Triplett, R.G., Nevins, M., Marx, R.E., Spagnoli, D.B., Oates, T.W., Moy, P.K., and Boyne, P.J. Pivotal, randomized, parallel evaluation of recombinant human bone morphogenetic protein-2/absorbable collagen sponge and autogenous bone graft for maxillary sinus floor augmentation. J Oral Maxillofac Surg **67,** 1947, 2009.
10. Govender, S., Csimma, C., Genant, H.K., Valentin-Opran, A., Amit, Y., Arbel, R., Aro, H., Atar, D., Bishay, M., Borner, M.G., Chiron, P., Choong, P., Cinats, J., Courtenay, B., Feibel, R., Geulette, B., Gravel, C., Haas, N., Raschke, M., Hammacher, E., van der Velde, D., Hardy, P., Holt, M., Josten, C., Ketterl, R.L., Lindeque, B., Lob, G., Mathevon, H., McCoy, G., Marsh, D., Miller, R., Munting, E., Oevre, S., Nordsletten, L., Patel, A., Pohl, A., Rennie, W., Reynders, P., Rommens, P.M., Rondia, J., Rossouw, W.C., Daneel, P.J., Ruff, S., Ruter, A., Santavirta, S., Schildhauer, T.A., Gekle, C., Schnettler, R., Segal, D., Seiler, H., Snowdowne, R.B., Stapert, J., Taglang, G., Verdonk, R., Vogels, L., Weckbach, A., Wentzensen, A., Wisniewski, T., and BMP-2 Evaluation in Surgery for Tibial Trauma (BESTT) Study Group. Recombinant human bone morphogenetic protein-2 for treatment of open tibial fractures: a prospective, controlled, randomized study of four hundred and fifty patients. J Bone Joint Surg Am **84-A,** 2123, 2002.
11. Calori, G.M., Tagliabue, L., Gala, L., d'Imporzano, M., Peretti, G., and Albisetti, W. Application of rhBMP-7 and platelet-rich plasma in the treatment of long bone nonunions: a prospective randomised clinical study on 120 patients. Injury **39,** 1391, 2008.
12. Giannoudis, P.V., and Tzioupis, C. Clinical applications of BMP-7: the UK perspective. Injury **36(Suppl 3),** S47, 2005.
13. Katayama, Y., Matsuyama, Y., Yoshihara, H., Sakai, Y., Nakamura, H., Imagama, S., Ito, Z., Wakao, N., Kamiya, M., Yukawa, Y., Kanemura, T., Sato, K., Iwata, H., and Ishiguro, N. Clinical and radiographic outcomes of posterolateral lumbar spine fusion in humans using recombinant human bone morphogenetic protein-2: an average five-year follow-up study. Int Orthop **33,** 1061, 2009.
14. Boerckel, J.D., Kolambkar, Y.M., Dupont, K.M., Uhrig, B.A., Phelps, E.A., Stevens, H.Y., Garcia, A.J., and Guldberg, R.E. Effects of protein dose and delivery system on BMP-mediated bone regeneration. Biomaterials **32,** 5241, 2011.
15. Carragee, E.J., Hurwitz, E.L., and Weiner, B.K. A critical review of recombinant human bone morphogenetic protein-2 trials in spinal surgery: emerging safety concerns and lessons learned. Spine J **11,** 471, 2011.
16. Zlotnik, A., and Yoshie, O. Chemokines: a new classification system and their role in immunity. Immunity **12,** 121, 2000.
17. Bleul, C.C., Farzan, M., Choe, H., Parolin, C., Clark-Lewis, I., Sodroski, J., and Springer, T.A. The lymphocyte chemoattractant SDF-1 is a ligand for LESTR/fusin and blocks HIV-1 entry. Nature **382,** 829, 1996.
18. Feng, Y., Broder, C.C., Kennedy, P.E., and Berger, E.A. HIV-1 entry cofactor: functional cDNA cloning of a seven-transmembrane, G protein-coupled receptor. Science **272,** 872, 1996.
19. Heesen, M., Berman, M.A., Benson, J.D., Gerard, C., and Dorf, M.E. Cloning of the mouse fusin gene, homologue to a human HIV-1 co-factor. J Immunol **157,** 5455, 1996.
20. Kucia, M., Jankowski, K., Reca, R., Wysoczynski, M., Bandura, L., Allendorf, D.J., Zhang, J., Ratajczak, J., and Ratajczak, M.Z. CXCR4-SDF-1 signalling, locomotion, chemotaxis and adhesion. J Mol Histol **35,** 233, 2004.
21. Granero-Molto, F., Weis, J.A., Miga, M.I., Landis, B., Myers, T.J., O'Rear, L., Longobardi, L., Jansen, E.D., Mortlock, D.P., and Spagnoli, A. Regenerative effects of transplanted mesenchymal stem cells in fracture healing. Stem Cells **27,** 1887, 2009.
22. Kitaori, T., Ito, H., Schwarz, E.M., Tsutsumi, R., Yoshitomi, H., Oishi, S., Nakano, M., Fujii, N., Nagasawa, T., and Nakamura, T. Stromal cell-derived factor 1/CXCR4 signaling is critical for the recruitment of mesenchymal stem cells to the fracture site during skeletal repair in a mouse model. Arthritis Rheum **60,** 813, 2009.
23. Otsuru, S., Tamai, K., Yamazaki, T., Yoshikawa, H., and Kaneda, Y. Circulating bone marrow-derived osteoblast progenitor cells are recruited to the bone-forming site by the CXCR4/stromal cell-derived factor-1 pathway. Stem Cells **26,** 223, 2008.
24. Zhu, W., Boachie-Adjei, O., Rawlins, B.A., Frenkel, B., Boskey, A.L., Ivashkiv, L.B., and Blobel, C.P. A novel regulatory role for stromal-derived factor-1 signaling in bone morphogenic protein-2 osteogenic differentiation of mesenchymal C2C12 cells. J Biol Chem **282,** 18676, 2007.
25. Hosogane, N., Huang, Z., Rawlins, B.A., Liu, X., Boachie-Adjei, O., Boskey, A.L., and Zhu, W. Stromal derived factor-1 regulates bone morphogenetic protein 2-induced osteogenic differentiation of primary mesenchymal stem cells. Int J Biochem Cell Biol **42,** 1132, 2010.
26. Higashino, K., Viggeswarapu, M., Bargouti, M., Liu, H., Titus, L., and Boden, S.D. Stromal cell-derived factor-1

potentiates bone morphogenetic protein-2 induced bone formation. Tissue Eng Part A **17,** 523, 2011.

27. Wise, J.K., Sumner, D.R., and Virdi, A.S. Modulation of stromal cell-derived factor-1/CXC chemokine receptor 4 axis enhances rhBMP-2-induced ectopic bone formation. Tissue Eng Part A **18,** 860, 2012.

28. Ratanavaraporn, J., Furuya, H., Kohara, H., and Tabata, Y. Synergistic effects of the dual release of stromal cell-derived factor-1 and bone morphogenetic protein-2 from hydrogels on bone regeneration. Biomaterials **32,** 2797, 2011.

29. Zhu, W., Liang, G., Huang, Z., Doty, S.B., and Boskey, A.L. Conditional inactivation of the CXCR4 receptor in osteoprecursors reduces postnatal bone formation due to impaired osteoblast development. J Biol Chem **286,** 26794, 2011.

30. Herberg, S., Fulzele, S., Yang, N., Shi, X., Hess, M., Periyasamy-Thandavan, S., Hamrick, M.W., Isales, C.M., and Hill, W.D. Stromal cell-derived factor-1beta potentiates bone morphogenetic protein-2-stimulated osteoinduction of genetically engineered bone marrow-derived mesenchymal stem cells *in vitro*. Tissue Eng Part A **19,** 1, 2013.

31. Katayama, Y., Battista, M., Kao, W.M., Hidalgo, A., Peired, A.J., Thomas, S.A., and Frenette, P.S. Signals from the sympathetic nervous system regulate hematopoietic stem cell egress from bone marrow. Cell **124,** 407, 2006.

32. Davis, D.A., Singer, K.E., De La Luz Sierra, M., Narazaki, M., Yang, F., Fales, H.M., Yarchoan, R., and Tosato, G. Identification of carboxypeptidase N as an enzyme responsible for C-terminal cleavage of stromal cell-derived factor-1alpha in the circulation. Blood **105,** 4561, 2005.

33. De La Luz Sierra, M., Yang, F., Narazaki, M., Salvucci, O., Davis, D., Yarchoan, R., Zhang, H.H., Fales, H., and Tosato, G. Differential processing of stromal-derived factor-1alpha and stromal-derived factor-1beta explains functional diversity. Blood **103,** 2452, 2004.

34. Marquez-Curtis, L., Jalili, A., Deiteren, K., Shirvaikar, N., Lambeir, A.M., and Janowska-Wieczorek, A. Carboxypeptidase M expressed by human bone marrow cells cleaves the C-terminal lysine of stromal cell-derived factor-1alpha: another player in hematopoietic stem/progenitor cell mobilization? Stem Cells **26,** 1211, 2008.

35. Stancoven, B.W., Lee, J., Dixon, D.R., McPherson, J.C., 3rd, Bisch, F.C., Wikesjo, U.M., and Susin, C. Effect of bone morphogenetic protein-2, demineralized bone matrix and systemic parathyroid hormone (1–34) on local bone formation in a rat calvaria critical-size defect model. J Periodontal Res **48,** 243, 2013.

36. Bouxsein, M.L., Boyd, S.K., Christiansen, B.A., Guldberg, R.E., Jepsen, K.J., and Muller, R. Guidelines for assessment of bone microstructure in rodents using micro-computed tomography. J Bone Miner Res **25,** 1468, 2010.

37. Ratajczak, M.Z., Serwin, K., and Schneider, G. Innate immunity derived factors as external modulators of the CXCL12-CXCR4 axis and their role in stem cell homing and mobilization. Theranostics **3,** 3, 2013.

38. Penn, M.S., Mendelsohn, F.O., Schaer, G.L., Sherman, W., Farr, M., Pastore, J., Rouy, D., Clemens, R., Aras, R., and Losordo, D.W. An open-label dose escalation study to evaluate the safety of administration of nonviral stromal cell-derived factor-1 plasmid to treat symptomatic ischemic heart failure. Circ Res **112,** 816, 2013.

39. Herberg, S., Shi, X., Johnson, M.H., Hamrick, M.W., Isales, C.M., and Hill, W.D. Stromal cell-derived factor-1beta mediates cell survival through enhancing autophagy in bone marrow-derived mesenchymal stem cells. PLoS One **8,** e58207, 2013.

40. Yun, J.I., Wikesjo, U.M., Borke, J.L., Bisch, F.C., Lewis, J.E., Herold, R.W., Swiec, G.D., Wood, J.C., and McPherson, J.C., 3rd. Effect of systemic parathyroid hormone (1–34) and a beta-tricalcium phosphate biomaterial on local bone formation in a critical-size rat calvarial defect model. J Clin Periodontol **37,** 419, 2010.

41. Bateman, J.P., Safadi, F.F., Susin, C., and Wikesjo, U.M. Exploratory study on the effect of osteoactivin on bone formation in the rat critical-size calvarial defect model. J Periodontal Res **47,** 243, 2012.

42. Spicer, P.P., Kretlow, J.D., Young, S., Jansen, J.A., Kasper, F.K., and Mikos, A.G. Evaluation of bone regeneration using the rat critical size calvarial defect. Nat Protoc **7,** 1918, 2012.

43. Wikesjo, U.M., Qahash, M., Polimeni, G., Susin, C., Shanaman, R.H., Rohrer, M.D., Wozney, J.M., and Hall, J. Alveolar ridge augmentation using implants coated with recombinant human bone morphogenetic protein-2: histologic observations. J Clin Periodontol **35,** 1001, 2008.

44. Wikesjo, U.M., Xiropaidis, A.V., Qahash, M., Lim, W.H., Sorensen, R.G., Rohrer, M.D., Wozney, J.M., and Hall, J. Bone formation at recombinant human bone morphogenetic protein-2-coated titanium implants in the posterior mandible (Type II bone) in dogs. J Clin Periodontol **35,** 985, 2008.

45. Wikesjo, U.M., Huang, Y.H., Xiropaidis, A.V., Sorensen, R.G., Rohrer, M.D., Prasad, H.S., Wozney, J.M., and Hall, J. Bone formation at recombinant human bone morphogenetic protein-2-coated titanium implants in the posterior maxilla (Type IV bone) in non-human primates. J Clin Periodontol **35,** 992, 2008.

46. Leknes, K.N., Yang, J., Qahash, M., Polimeni, G., Susin, C., and Wikesjo, U.M. Alveolar ridge augmentation using implants coated with recombinant human bone morphogenetic protein-2: radiographic observations. Clin Oral Implants Res **19,** 1027, 2008.

47. De Clercq, E., Yamamoto, N., Pauwels, R., Balzarini, J., Witvrouw, M., De Vreese, K., Debyser, Z., Rosenwirth, B., Peichl, P., Datema, R., and *et al.* Highly potent and selective inhibition of human immunodeficiency virus by the bicyclam derivative JM3100. Antimicrob Agents Chemother **38,** 668, 1994.

48. Broxmeyer, H.E., Orschell, C.M., Clapp, D.W., Hangoc, G., Cooper, S., Plett, P.A., Liles, W.C., Li, X., Graham-Evans, B., Campbell, T.B., Calandra, G., Bridger, G., Dale, D.C., and Srour, E.F. Rapid mobilization of murine and human hematopoietic stem and progenitor cells with AMD3100, a CXCR4 antagonist. J Exp Med **201,** 1307, 2005.

Address correspondence to:
William D. Hill, PhD
Department of Cellular Biology and Anatomy
Georgia Regents University
CB-1119, 1459 Laney Walker Blvd.
Augusta, GA 30912

E-mail: whill@gru.edu